https://doi.org/10.2352/ISSN.2470-1173.2018.15.COIMG-133

Data-driven Compressed Sensing Tomography

Marc Kassubeck, Stephan Wenger; TU Braunschweig; Braunschweig, Niedersachsen/Germany
Chris A. Jennings, Matthew Gomez, Eric Harding, Jens Schwarz; Sandia National Laboratories; Albuquerque; New Mexico/USA
Marcus Magnor; TU Braunschweig; Braunschweig, Niedersachsen/Germany

Abstract

This paper presents a new method for tomographic reconstruction of volumes from sparse observational data. Application scenarios can be found in astrophysics, plasma physics, or whenever the amount of obtainable measurement is limited. In the extreme only a single view of the phenomenon may be available. Our method uses input image data together with complex, user-definable assumptions about 3D density distributions. The parameter values of the user-defined model are fitted to the input image. This allows for incorporating complex, data-driven assumptions, such as helical symmetry, into the reconstruction process. We present two different sparsity-based reconstruction approaches. For the first method, novel virtual views are generated prior to tomography reconstruction. In the second method, voxel groups of similar target densities are defined and used for group sparsity reconstruction. We evaluate our method on real data of a high-energy plasma experiment and show that the reconstruction is consistent with the available measurement and 3D density assumptions. An additional experiment on simulated data demonstrates possible gains when adding an additional view to the presented reconstruction methods.

Introduction

Tomographic reconstruction [7] is a method to obtain information about the internal structure of objects non-invasively. It is a well established approach in the context of measuring transmissive as well as emissive density distributions of an object. As such it is able to reveal material properties in the transmissive case or radiation distributions like the energy content of a heated plasma in the emissive case. This property makes it a useful tool in many application areas, including but not limited to: radiology, archeology, geophysics, astrophysics and plasma physics. Tomographic reconstruction in a classical sense requires data from many different projectional measurements to compute a full reconstruction. However, there exist application areas, which make the acquisition of the required amount of measurement data very costly or even impossible. An example of such an application is fusion research at Sandia National Laboratories (SNL).

SNL performs research in Inertial Confinement Fusion (ICF) using an approach called Magnetized Liner Inertial Fusion (MagLIF) [5]. To this end, deuterium gas inside a Beryllium cylinder is heated by a laser and compressed by a magnetic field resulting from a high current flowing through the surrounding metal tube. An additional axial magnetic field confines the plasma along the cylinder axis which prevents heat loss. Figure 1 shows a false colored measurement of x-ray radiation emerging from the heated plasma. Experiments and diagnostics are very costly, as experiment setup and cleanup takes approximately one day and diagnostic components are destroyed. This results in a severe limitation of the number of shots and the amount of diagnostics.

Compressed sensing [3, 4] describes conditions, which allow for perfect signal reconstruction with only a small number of measurements. One important condition is the sparsity of the signal in a specific space. We will show that even if this condition is not perfectly fulfilled for the given data, the reconstruction is still robust enough to generate convincing visualizations. The task in this paper is the reconstruction of a plausible volumetric density distribution explaining the x-ray emission of a MagLIF plasma from as few as just a single image. The input to the presented algorithm is the measured x-ray image and a user-specified parametric 3D density distribution model, which does not require additional knowledge of the underlying physical phenomenon. The desired output is a plausible volume, which aims to conform to both measurement and model.

Related Work

Tomographic reconstruction has been an active research field with algebraic reconstruction methods dating back almost 50 years [6]. As such there have been numerous fundamental works on this topic. For the case of (medical) computed tomography [7] gives an overview of current practices.

Tomographic reconstruction has also been successfully applied in the context of measuring plasma experiments. The authors of [11] discuss several inversion techniques with respect to fast computation time and application to tokamak reactors and [9] adapts Phillips-Tikhonov regularization to tokamak plasmas and evaluates robustness against the presence of noise.

Compressive sensing [4] methods are a family of established signal reconstruction techniques, which have been successfully applied to problems such as image reconstruction under missing pixel information [10].

The works most related to ours are [14, 15]. Both focus on volumetric reconstruction in the context of planetary nebulae, with axial and spherical symmetries using only one image. They provide the basic optimization framework for our investigation, which we extend with a consistent formulation for multiple projections and our data-driven symmetry constraints.

Method

One key concept in tomography is the reconstruction of a 3D density function $\rho : \mathbb{R}^3 \supset \Omega \to \mathbb{R}$ from a set of 2D projections $s : \mathbb{R}^2 \supset \Pi \to \mathbb{R}$. An example of one such projection is the integration over the z-axis of the 3D density or the summation in the discrete case

$$s(x,y) = \int_z \rho(x,y,z)\,\mathrm{d}z \quad \text{or} \quad s(x,y) = \frac{1}{\sqrt{n_z}} \sum_z \rho(x,y,z) \quad (1)$$

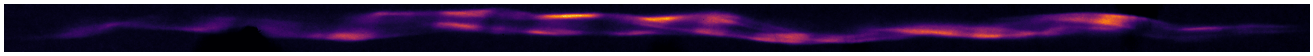

Figure 1. *The false colored measurement of x-ray radiation emerging from the heated plasma at the point of stagnation.*

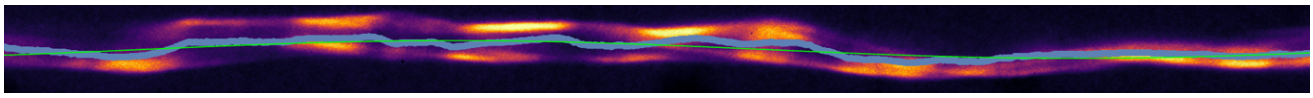

Figure 2. *Central crop of input. Blue marks intensity centroids and green the fit of a general helix to centroid data.*

with n_z being the number of voxels in direction of the z-axis. Note that in this case the voxel grid is aligned to the image grid and the normalization by $\sqrt{n_z}$ bears no physical significance, but improves convergence of the algorithm adopted below.

The general form of this projection is to assume that the sensor response can be modeled as a linear map acting on ρ, which is true for many real-world cases. In the discrete case P becomes a matrix, which maps a voxel grid with dimensions $i \times j \times k$ to pixel space $u \times v$:

$$s = P\rho, \quad \text{with} \quad P \in \mathbb{R}^{ijk \times uv} \tag{2}$$

This matrix is usually sparsely populated, as each row only contains non-zero weights for the voxels that are hit by the ray through the corresponding pixel in the image plane. Given a set of such projection matrices $\mathbf{P} = \{P_i : i = 1 \dots n\}$ with corresponding sensor data $\mathbf{s} = \{s_i : i = 1 \dots n\}$ one can formulate the problem of reconstructing the generating density ρ as minimization of the following energy term:

$$D_{\mathbf{P},\mathbf{s}}(\rho) = \frac{1}{2} \sum_{i=1}^{n} \|P_i\rho - s_i\|_2^2 \tag{3}$$

Minimizing $D_{\mathbf{P},\mathbf{s}}(\rho)$ is equivalent to a linear least squares problem argmin $\frac{1}{2}\|Ax-b\|_2^2$. The system matrix A and the right hand side b correspond to the stacked projection matrices and sensor measurements:

$$A = (P_1, P_2, \dots, P_n)^T, \quad b = (s_1, s_2, \dots, s_n)^T \tag{4}$$

In usual tomographic reconstruction applications the number of projections are selected to obtain a nearly square matrix A. More projections lead to an overdetermined system, which increases computation time while not necessarily improving reconstruction accuracy. Less projections lead to an underdetermined system, which permits a whole subspace of possible solutions.

However, this poses a problem, when the number of obtainable views is limited. We present two methods to incorporate additional knowledge of symmetry properties of the density distribution into the reconstruction and improve the reconstruction even in the extreme case of only one available projection.

Virtual view reconstruction

The first method we propose, is based on the idea that it is possible to generate novel virtual views of the volume by image based transformations of given views and placement of virtual camera positions. Given a sparse set of input measurements $\tilde{\mathbf{s}}$ with accompanying projections $\tilde{\mathbf{P}}$, we can generate a new set of inputs $\mathbf{s} \supset \tilde{\mathbf{s}}, \mathbf{P} \supset \tilde{\mathbf{P}}$ to minimize equation 3.

In case of approximately helical symmetry this corresponds to placing new virtual views around the axis of the helix, see

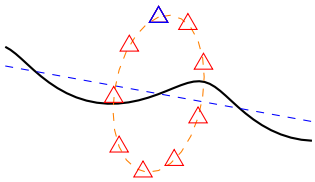

Figure 3. *Novel view generation based on one input view (blue triangle). Novel views (red triangles) are generated by shifting input measurements with respect to the helix pitch.*

figure 3. Assuming orthographic projections, novel virtual sensor measurements are blended and shifted versions of the original measurements. Given two original camera views $\tilde{s}_1, \tilde{s}_2$ on the circle, we compute an in-between views with position $t \in [0,1]$

$$s_t = t\phi(\tilde{s}_1, \lambda, t) + (1-t)\phi(\tilde{s}_2, \lambda, 1-t), \tag{5}$$

with ϕ being the shift of an image in direction of the helix' axis. The parameter λ describes the pitch of the helix. We derive it from image data by first computing the intensity centroids perpendicular to the axis of the helix in the image plane. Afterwards we fit the parameters a, b, c of a general helix $(bx, a\sin(x) + c, a\cos(x) + c)^T$ to these centroids using non-linear least squares optimization. See figure 2 for the fitting result on measured data.

Finally, we add a ℓ_1 regularization term to the optimization:

$$R_1(\rho) = \|\rho\|_1 \tag{6}$$

This term promotes the sparsity of the solution [2], i.e. a solution with few high-density voxels and the rest close to zero.

We use the method of [14] for optimization of the combined energy with $\tau > 0$ being a weight to control the influence of the regularization term:

$$\begin{aligned} &\operatorname*{argmin}_{\rho} D_{\mathbf{P},\mathbf{s}}(\rho) + \tau R_1(\rho) \\ &s.t.\ \rho \geq 0 \\ &s.t.\ B\rho = c \end{aligned} \tag{7}$$

The optional hard constraints $B\rho = c$ enforce stronger adherence to views that are known to be correct, i.e. the input views. We set B and c as follows:

$$B = (\tilde{P}_1, \dots, \tilde{P}_k)^T,\ \tilde{P}_i \in \tilde{\mathbf{P}}, \quad c = (\tilde{s}_1, \dots, \tilde{s}_k)^T,\ \tilde{s}_i \in \tilde{\mathbf{s}} \tag{8}$$

Unless noted differently we use $\tau = 1$ and $n_g = 50$ virtual cameras arranged in a half circle around the axis of the helix for our experiments.

Group sparsity reconstruction

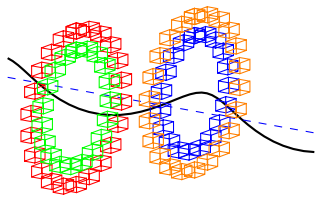

Figure 4. *Voxel groups are concentric rings perpendicular to the axis of the helix with centers derived from intensity centroids (e.g. red, green, blue, orange).*

Our second method also uses the data term from equation 3, but instead of filling missing information by image transformations we construct a stronger regularization term, which is able to resolve the ambiguity in solution space due to missing data.

We achieve this by defining voxel groups, i.e. sets of voxels which we assume to have the same density value. These groups are pairwise disjoint and form a full partition of the voxel grid.

In case of approximately helical symmetry we again start by computing intensity centroids of the image data (figure 2). If we can locate the centroids in 3D space (e.g. using two orthogonal measurements) we use these as centers for concentric rings to form our voxel groups (figure 4).

If we can't fully locate the centroids (e.g. if only one projection is available) we fit a generic helix trajectory to the centroids as in the previous section. The ring centers are then shifted in the planes, which provide centroid data to better fit our model to the measurements.

Let $\mathbf{G} = \{G_j, j = 1,\ldots,n_g\}$ denote the set of voxel groups. We define $\rho_{\{G_j\}} = \{\rho(x,y,z) : (x,y,z) \in G_j\}$ as the set of densities of group G_j. With this we define our group sparsity regularizer as:

$$R_2(\rho) = \sum_j |G_j| \max \rho_{\{G_j\}} \tag{9}$$

This regularizer is a weighted $\ell_{1,\infty}$ norm over all groups under the constraint that $\rho \geq 0$ everywhere, which is enforced in equation 10. The regularizer penalizes each group with the maximum value of that group, which enforces concentration of intensity values to as few groups as possible, while also requiring similar intensity values in each group.

The scaling with the number of voxels in each group $|G_j|$ is necessary to prevent accumulation of densities in larger groups (in rings with larger radii). Without this term it would be possible to deposit densities in these groups and not incur any penalization, as only the largest value in each group would be taken into account.

We use the method detailed in [15] to optimize the combined energy with $\tau > 0$ as a user-defined weight to control the influence of the regularizer:

$$\begin{aligned} &\operatorname*{argmin}_{\rho} D_{\mathbf{P},\mathbf{s}}(\rho) + \tau R_2(\rho) \\ &s.t.\ \rho \geq 0 \end{aligned} \tag{10}$$

Unless noted differently we use $\tau = 0.1$ in our experiments.

Results

We evaluate our reconstruction methods on synthetic as well as real measurement data.

All algorithms are performed on a workstation computer with an *Intel Core i7 6700k, 4×4GHz* CPU with an *NVIDIA GTX 970* GPU and *32 Gb* of RAM.

The real-world data consists of one measurement of x-ray radiation of an imploding MagLIF plasma at stagnation (see figure 2) with resolution of 1999×123 pixels and 16 bit per pixel depth. This resulted in a volume of size $1999 \times 123 \times 123$ voxels. The computation with the virtual view reconstruction took approximately 14 hours and the group sparsity reconstruction took approximately 20 minutes.

Figure 5 and 6 show projections of the reconstructed volume with both algorithms. It is observable that group sparsity reconstruction more faithfully represents the input (0°) view than virtual view reconstruction, which tends to introduce blurry streaks. The orthogonal (90°) projections of both methods reveal further artifacts. In this case the virtual view reconstruction is even more blurred and group sparsity reconstruction shows a projection, which is too symmetric to be physically plausible, but looks convincing to human perception because of strong locality of the emissive volume.

To better estimate the quality of the reconstruction, we conducted further tests on synthetic ground truth data of a numerical simulation (figure 7) of the underlying physical process — see [8] for an introduction. Availability of ground truth data allows us to test the algorithms with varying number of input views — only one and two orthogonal views in our case. The simulated and reconstructed volumes are of size $832 \times 38 \times 38$ voxels. Computation times for this small volume were around 20 minutes for virtual view and 30 seconds for group sparsity reconstruction.

To estimate the quality of the reconstruction, we compute the error of several 2D projections of the reconstructed and ground truth volume at different camera positions as well as the error of the full 3D volume. The following table shows the peak signal-to-noise ratio (PSNR) of these errors. The projections mentioned in this table can be seen in figures 7 – 11. Unsurprisingly, the addition of an orthogonal view improves the reconstruction quality by a significant amount.

Comparison	1 view		2 views	
	VV	**GS**	**VV**	**GS**
0° proj.	35.44	**47.60**	37.14	44.11
90° proj.	27.93	29.53	37.25	**45.97**
45° proj.	28.90	31.42	32.24	**33.67**
full volume	37.48	38.11	**40.01**	39.75

PSNR values (in dB) for the reconstruction of simulated data with virtual view (VV) and group sparsity (GS) with a single projection and two orthogonal projections as input.

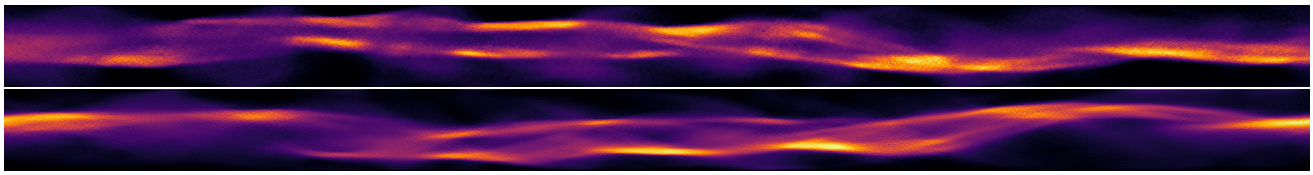

Figure 5. *Reconstruction of measurement using virtual view reconstruction. Input to the reconstruction is shown in figure 2. Top: Input view of reconstructed volume, bottom:* 90° *view of reconstructed volume*

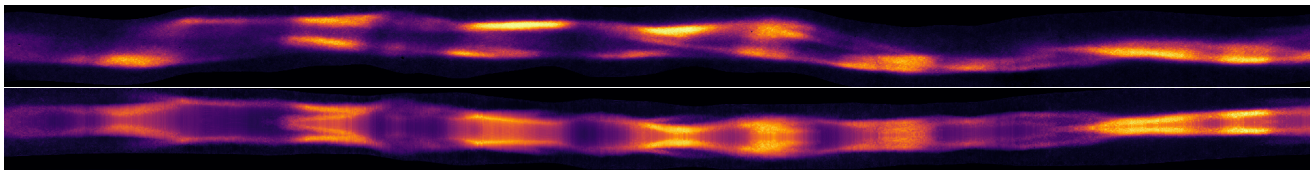

Figure 6. *Reconstruction of measurement using group sparsity reconstruction. Input to the reconstruction is shown in figure 2. Top: Input view of reconstructed volume, bottom:* 90° *view of reconstructed volume*

Surprisingly, virtual view reconstruction seems to outperform group sparsity reconstruction in the full 3D comparison, when two orthogonal views are available, even though it is outperformed in every single projection case. This shows the ambiguity that is present, when trying to explain a 3D volume by only three 2D projections of this volume. Also note that these experiments were conducted on a single synthetic example, which is insignificant in deciding, which algorithm outperforms the other. The examples are meant to show that both algorithms produce visually plausible results that can be generated using moderate computational resources. Furthermore both methods require only little user input by setting some global parameters like the regularization strength or the number of virtual views.

All reconstructed volumes mentioned here (and shown in figures 5 – 11) can be viewed as rotating projections on the project website [1] to gain more intuitive insight into local differences of the full 3D density distributions.

Conclusion

We have presented a novel approach for reconstruction of approximately symmetric 3D density data from as few as only one projection. Our results indicate that it is possible to obtain visually pleasing results, which reproduce the measurement data faithfully. Tests on simulated data further reveal how much information can be gained from expanding a single line of sight measurement with a second orthogonal line of sight measurement.

The reconstruction of a physically plausible volume is still an open problem. It is conceivable that better reconstruction results are possible when incorporating further knowledge of the process of the physical system into the reconstruction. Our further work shall investigate, whether additional regularizers can be derived from simulation or successive measurement and utilized as a prior for reconstruction. In this context machine learning and especially neural network approaches could prove a useful tool for regressing a strong model, which generalizes well to unseen data. Another interesting approach could be the incorporation of time gated measurements, which allow utilization of the time evolution of the imploding plasma into the reconstruction to resolve the issue of ambiguity in the solution space.

[1] `https://graphics.tu-bs.de/publications/kassubeck2018data-driven`

Acknowledgments

This work was supported by a travel grant from Sandia National Laboratories.

Sandia National Laboratories is a multimission laboratory managed and operated by National Technology and Engineering Solutions of Sandia, LLC, a wholly owned subsidiary of Honeywell International, Inc., for the U.S. Department of Energy's National Nuclear Security Administration under contract DE-NA0003525.

References

[1] Amir Beck, et. al., A fast iterative shrinkage-thresholding algorithm for linear inverse problems, SIAM journal on imaging sciences, pg. 183. (2009).

[2] Richard G. Baraniuk, Compressive sensing [lecture notes], IEEE signal processing magazine, pg.118. (2007).

[3] Emmanuel J. Candès, et al., Stable signal recovery from incomplete and inaccurate measurements, Communications on Pure and Applied Mathematics, pg. 1207. (2006).

[4] David L. Donoho, Compressed sensing, IEEE Transactions on Information Theory, pg. 1289. (2006).

[5] Matthew Gomez, et. al., Demonstration of thermonuclear conditions in magnetized liner inertial fusion experiments, Physics of Plasmas, pg. 056306. (2015).

[6] Richard Gordon, et. al., Algebraic reconstruction techniques (ART) for three-dimensional electron microscopy and x-ray photography, Journal of theoretical Biology, pg. 471IN1477. (1970).

[7] Jian Hsieh, et. al., Computed tomography: principles, design, artifacts, and recent advances. (2009).

[8] Chris A. Jennings, et. al., Simulations of the implosion and stagnation of compact wire arrays, Physics of Plasmas, pg. 092703. (2010)

[9] Seung H. Lee, et al., Modified Phillips-Tikhonov regularization for plasma tomography, Current Applied Physics, pg. 893. (2010).

[10] Xiaoyang Liu, et. al., Compressive Volume Rendering, Computer Graphics Forum, pg. 101. (2015).

[11] Jan Mlynar, et. al., Inversion techniques in the soft-x-ray tomography of fusion plasmas: Toward real-time applications, Fusion Science and Technology, pg. 733. (2010).

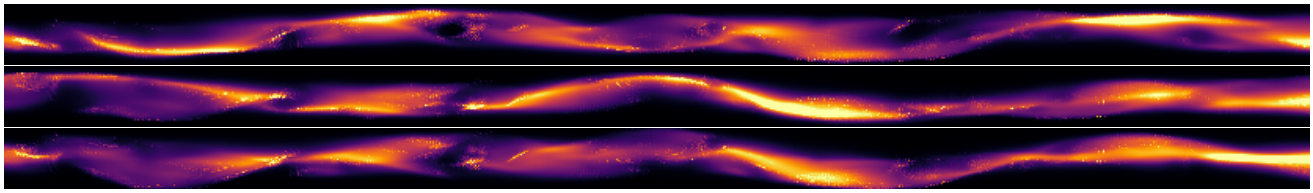

Figure 7. *Ground truth projections of simulation data. Top: projection with $0°$, middle: projection with $90°$, bottom: projection with $45°$ rotation around helix axis.*

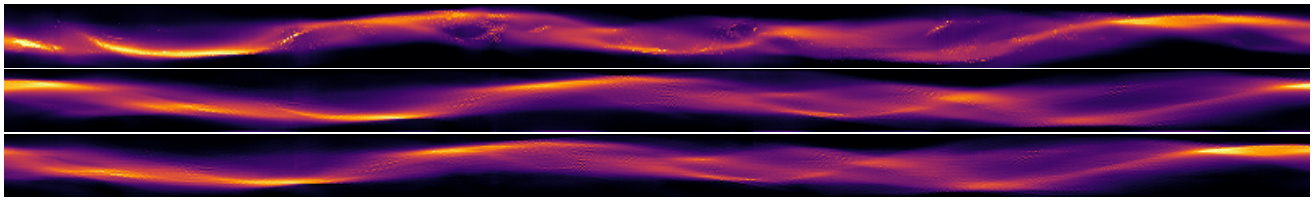

Figure 8. *Virtual view reconstruction of simulation data with one projection ($0°$ in figure 7) as input. Top: projection with $0°$, middle: projection with $90°$, bottom: projection with $45°$ rotation around helix axis.*

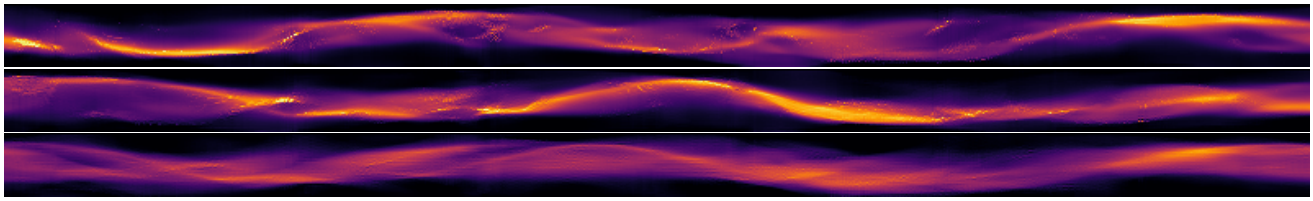

Figure 9. *Virtual view reconstruction of simulation data with two orthogonal projections ($0°$ and $90°$ see figure 7) as input. Top: projection with $0°$, middle: projection with $90°$, bottom: projection with $45°$ rotation around helix axis.*

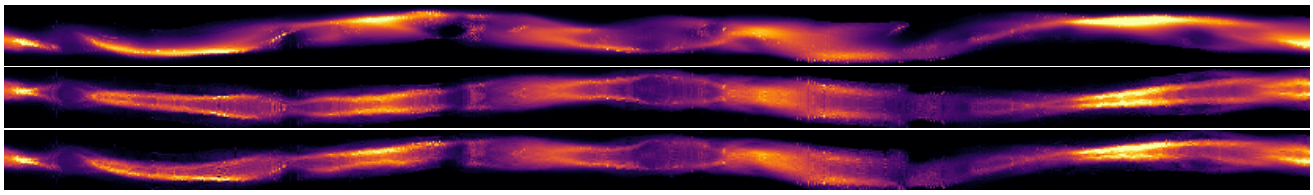

Figure 10. *Group sparsity reconstruction of simulation data with one projection ($0°$ in figure 7) as input. Top: projection with $0°$, middle: projection with $90°$, bottom: projection with $45°$ rotation around helix axis.*

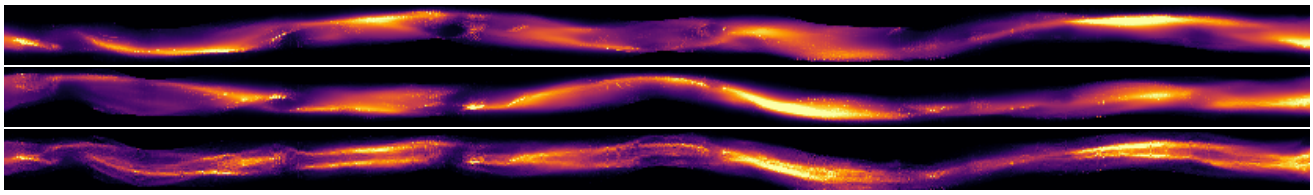

Figure 11. *Group sparsity reconstruction of simulation data with two orthogonal projections ($0°$ and $90°$ see figure 7) as input. Top: projection with $0°$, middle: projection with $90°$, bottom: projection with $45°$ rotation around helix axis.*

[12] Michal Odstrcil, et. al., Modern numerical methods for plasma tomography optimisation, Nuclear Instruments and Methods in Physics Research Section A: Accelerators, Spectrometers, Detectors and Associated Equipment, pg. 156. (2012).
[13] Stephan Wenger, et. al., Algebraic 3D reconstruction of planetary nebulae, Journal of WSCG, pg.33. (2009).
[14] Stephan Wenger, et. al., Visualization of astronomical nebulae via distributed multi-gpu compressed sensing tomography, IEEE transactions on visualization and computer graphics, pg. 2188. (2012).
[15] Stephan Wenger, et. al., Fast Image-Based Modeling of Astronomical Nebulae, Computer Graphics Forum, pg. 93. (2013).
[16] J.H. Williamson, et. al., Computerized Tomography for Sparse-Data Plasma Physics Experiments, IEEE Transactions on Plasma Science, pg. 82. (1982).

Author Biography

Marc Kassubeck received his master's degree in computer science in 2016 from TU Braunschweig, Germany. He is currently pursuing his Ph.D. in computer graphics at TU Braunschweig, Germany. His research interests include image and volume processing, inverse problems and machine learning.

Dr. Stephan Wenger received his master's degrees in physics and computer science as well as his Ph.D. in computer graphics from TU Braunschweig. His areas of interest include mathematical optimization, compressed sensing, volumetric reconstruction, computational astronomy, image-based reconstruction, audio processing, physics simulation, and parallel computing. He is now a senior software engineer at Google Zurich.

Dr. Chris A. Jennings received the M.Sci. degree in physics and the Ph.D. degree in computational modeling of wire-array Z-pinches imploded by multi-mega-ampere currents from Imperial College London, London, U.K., in 2005. Since 2006, he has worked at Sandia National Laboratories, Albuquerque, NM, where he is currently with the ICF target design group. He has continued to work on the computational modeling of wire-array Z-pinches, gas puffs, and metallic liner implosions (MagLIF).

Dr. Matthew Gomez earned the Doctorate degree in Nuclear Engineering and Radiological Sciences from the University of Michigan in 2011. Matthew is currently a staff member at Sandia National Laboratories, where he studies inertial confinement fusion and high energy density science on the Z machine. Matthews research interests include magneto-inertial fusion sources, power flow and current coupling in large pulsed power drivers, and x-ray diagnostic development.

Dr. Jens Schwarz received his Ph.D. in Physics in 2003 for his work on ultra-short UV laser pulse propagation through the atmosphere. Since then, he has been working on PW class laser systems within the field of high energy density science and inertial confinement fusion.

Prof. Marcus Magnor heads the Computer Graphics Lab at Braunschweig University of Technology, Germany, and is adjunct faculty at the University of New Mexico, USA. He holds degrees in physics, electrical engineering, and computer science. His research interests include, but are not limited to, computer graphics, computer vision, visual perception, image processing, computational photography, astrophysics, imaging, optics, visual analytics, and visualization.